Experimental Mechanics (2019) 59:883–897
https://doi.org/10.1007/s11340-018-00467-y

Effect of Filling Pattern on the Tensile and Flexural Mechanical Properties of FDM 3D Printed Products

B. Akhoundi[1] · A.H. Behravesh[1]

Received: 26 June 2018 / Accepted: 18 December 2018 / Published online: 17 January 2019

Abstract

This experimental study investigates the effect of filling pattern on tensile and flexural strength and modulus of the parts printed via fused deposition modeling (FDM), 3D printer. The main downside of the printed products, with an FDM 3D printer, is the low strength compared to the conventional processes such as injection molding and machining. The issue stems from the low strength of thermoplastic materials and the weak bonding between deposited rasters and layers. Selection of proper filling pattern and infill percentage could highly influence the final mechanical properties of the printed products that were experimentally explored in this research work. Concentric, rectilinear, hilbert curve, and honeycomb patterns and filling percentage of 20, 50 and 100 were the variable parameters to print the parts. The results indicate that concentric pattern yields the most desirable tensile and flexural tensile properties, at all filling percentages, apparently due to the alignment of deposited rasters with the loading direction. Hilbert curve pattern also yielded a dramatic increase in the properties, at 100% filling. The dramatic increase could be mainly attributed to the promotion of strong bonding between the rasters and layers, caused by maintaining a high temperature of rasters at short travelling distances of nozzle for the hilbert curve pattern. Scanning electron microscopy (SEM) examination revealed the strong bonding between rasters and sound microstructures (less flaws and voids) for concentric and hilbert curve pattern at a high filling percentage of 100. Besides, SEM examination revealed large voids in honeycomb pattern, deemed to be responsible for its lower strength and modulus, especially at the filling percentage of 100.

Keywords FDM 3D printer · Fill pattern · Fill percentage · Mechanical properties · FDM parameters

Introduction

In the recent decade, remarkable progresses have been observed in additive manufacturing (AM) processes, in various aspects including materials, equipment, and processes. In AM, the printed product consists of the layers that are bonded together to form the final part [1, 2]. Among AM processes, FDM has become attractive to industry and public due to its simplicity and low-cost. While, it is mainly employed for manufacturing, rapid prototyping and rapid tooling [3], the use of FDM in different fields such as medical and dentistry [4–6], consumer products [7] and food industry [8] has been found promising. Due to the nature of forming layer-by- layer, that is the main feature of an AM process, the strength of the products printed by FDM method is lower compared to the conventional processes such as machining and injection molding [9]. The printed part in FDM 3D printer is, in essence, an orthotropic material where the properties in raster direction are deemed to be different from that of transverse direction. The complexity is added by considering the partial bonding between rasters and layers, and the existence of the voids that are created in the region of bonding between rasters and layers [10]. Therefore, each printed part is made of layers, and each layer is made of rasters. The two key factors that govern mechanical properties of the parts produced via FDM are: 1) quality of bonds between rasters and layers, and 2) content of voids (size and population). In other words, by improving the quality of the bonds between rasters and layers [11], and by reducing the quantity and sizes of the voids, mechanical properties would experience significant improvements. The quality of bonds and the characteristics of voids are the functions of FDM parameters. These parameters include nozzle temperature, envelope temperature, layer height, nozzle diameter, extrusion width, air gap, build

✉ A. H. Behravesh
amirhb@modares.ac.ir

[1] Additive Manufacturing Laboratory, Faculty of Mechanical Engineering, Tarbiat Modares University, Jalaal-e Al-Ahmed ExpWay, Tehran 14115-143, Iran

direction, print orientation, raster orientation, raster angle, filling pattern, and filling percentage. All of these parameters affect the quality of bonding between layers and rasters and determine the quantity of voids in the final product.

Numerous researches have been conducted to investigate the effect of process parameters on the strength of printed parts using FDM process. Ahn et al. [12] studied the tensile strength of printed ABS parts. They investigated the effects of raster orientation, air gap, raster width, color, and nozzle temperature parameters. By negative air gap and raster angle of 0^o, the obtained tensile strength increased up to72% of the tensile strength yielded with an injection molded part. Panda et al. [13] simulated FDM process parameters and their effects on tensile, flexural, and impact strengths. They applied bacterial foraging technique and studied the effects of layer height, part orientation, raster angle, bead width, and air gap parameters in different levels. They stated that thick rasters results in a high temperature near the bonding surfaces which may improve the diffusion and may result in strong bond formation. Rayegani and Onwubola [14] worked on modeling, predicting, and optimization of FDM process parameters by deploying the group method for data handling (GMDH) and differential evolution (DE). The most important factor affecting the strength was the air gap, so that, by negative air gap, the highest tensile strength was resulted. Tymrak et al. [15] investigated the mechanical properties of printed parts made of ABS and PLA. The variable parameters were $0/90^o$ and + 45/−45 filling patterns, 0.2, 03, and 0.4 mm layer heights, for 100% filling percentage. For ABS, the maximum strength of 25.5 MPa was obtained as with 0.2 mm layer height and + 45/−45 filling pattern and for PLA, the maximum strength was 56.6 MPa in 0.2 mm layer height and 0/90 filling pattern. Malenka et al. [16] studied the tensile properties of the printed PLA parts. Results showed that the tensile strength and modulus in 90^o orientation was higher compared to those of 45^o orientation. By increasing filling percentage from 10% to 80% the tensile strength and modulus increased. Moreover by increasing the layer height from 0.1 mm to 0.25 mm, the tensile strength and modulus decreased. Torres et al. [17] studied the effects of layer height, filling percentage, and heat treatment time at $100^{\circ}C$, on shear strength of the printed PLA parts. Improvement in shear strength was resulted by reducing the layer height, increasing the filling percentage and the duration of heat treatment. Baich et al. [18] studied the effects of filling patterns on strength and cost of the printed parts. They investigated the effects of filling patterns including low, high, double dense, and solid. The maximum tensile, compressive and flexural strengths and modulus were resulted in the solid samples. Fernandez-Vicente et al. [19] studied the effects of filling patterns and the filling percentage on tensile strength of printed ABS parts. The maximum tensile strength was obtained around 36.6 MPa in rectilinear pattern and 100% filling percentage. Dawoud et al. [20] studied the mechanical properties of printed parts by varying the parameters including air gap and raster angle. By negative air gap, the bulk density of the printed parts became more similar to those of injected parts, thus, an increase in strength was resulted. Wang et al. [21] added micro-spheres that could expand by the applied heat to the polymer in order to eliminate the voids in the printed part, that could improve the mechanical properties. By using 2 wt% of the microspheres and the heat treatment at $140^{\circ}C$ for 120 s, not only the voids reduced, but also tensile and compressive strength increased by 25.4% and 52.2%, respectively. Mohemad et al. [22], employed the blend of PC and ABS, in order to utilize the advantages of both materials in terms of properties and process. They studied the effects of layer height, air gap, raster angle, part orientation, bead width, and number of perimeters on time dependent mechanical properties. The amount of creep reduced by reducing layer height, air gap, and raster angle and increased by increasing the part orientation, bead width and number of perimeters.

The literature survey indicated that, while a large spectrum of filling patterns have been introduced, no comprehensive comparison has been reported. The main purpose of this research work was to extensively study the effect of filing pattern on mechanical properties of FDM printed parts. Selection of an appropriate filling pattern, due to the existence of many suggested ones, is an important step in sound production of parts in the relevant 3D printer (FDM, SLA, SLM, for instance). Therefore, it remains uncertain what strategy to apply to serve the purpose. On the other hand, mechanical-wise, the 3D printed parts, especially FDM parts, suffer from weaker strengths and stiffness, in comparison to the plastic injected molded counterparts. Therefore, one ultimate purpose is to achieve higher strength and stiffness in the final FDM products. The argument above results in a need to obtain the proper filling pattern(s), among the existing filling strategies, that is superior for achieving higher mechanical properties. The authors continued to investigate this issue and explored the fundamental(s) of the differences, by considering the impact on thermal history and size of the voids. Also, the correlation between mechanical properties and the microstructures of the printed parts was explored, in order to present an extensive experimental study from a mechanical point of view.

Deposition Scheme in FDM Process

In FDM process, filament shaped thermoplastic materials are heated up to a temperature at which the material can be extruded through a nozzle. Extruded materials, called rasters, are deposited next to each other to create a layer [9]. The final product is the result of many layers bonded together. The printed products via FDM process is an orthotropic material characterized by partial bonding between the rasters, partial bonding between the layers, and presence of voids [10]. These voids are created between rasters and layers, most often inevitably (Fig. 1).

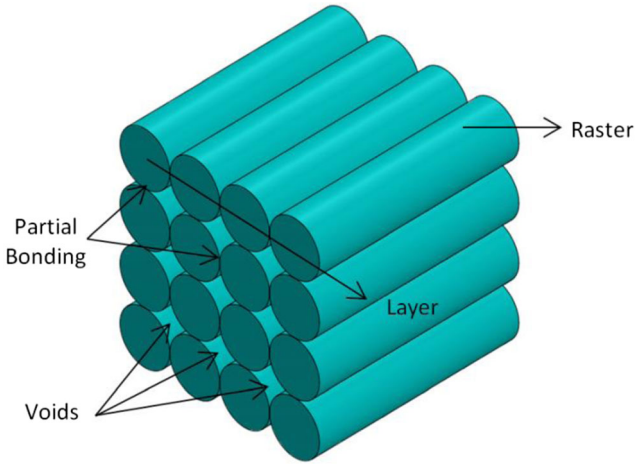

Fig. 1 A schematic of FDM deposition: Rasters, layers, voids, and partial bonding

The main parameters in FDM process include nozzle temperature, envelope temperature, layer height, nozzle diameter, extrusion width, air gap, build direction, part or rater orientation, raster angle, filling pattern, and filling percentage. All of these parameters could affect the strength by affecting thermal history and size of voids.

Temperature Since the bonding between the rasters and layers are promoted by thermal energy of semi-molten materials, thermal history of the polymeric raster plays a pivotal role in quality of bonding [10]. Conduction is the dominant heat transfer mechanism between the layers and rasters, and between bed and the first layer. In addition, rasters and layers are exposed to the ambient, and thus, experience convection mode of heat transfer (Fig. 2). When the heat transfer to the ambient is insignificant, and the table and nozzle temperatures are sufficiently high, the bonding between rasters and layers is expected to be stronger. This would lead to an increase in mechanical properties of final printed product. Post-heat treatment could be also followed to strengthen the thermal bonding between the rasters and layers [17].

Layer Height and Extrusion Width If the layer height is selected the same as the nozzle diameter, the cross sections of the rasters remain circular, and the voids in the final product will be larger (Fig. 1). In order to reduce the size of voids, the layer height can be varied as a key printing parameter; the lower the layer height, the smaller the void size. The compromise is that by reducing the layer height, the printing time increases. When the layer height is less than the nozzle diameter, the cross section of the raster deforms to a rectangular shape with round corners [9]. In this case, the rectangle width and height are called "extrusion width" and "layer height", respectively (Fig. 3(a)). The appropriate extrusion width is adjusted between the inner and outer diameter of nozzle. Inner feature is the orifice and the outer feature is the flat end of the nozzle (Fig. 3(b)). With an increase in extrusion width, the radius at the corners increases and, consequently, the size of voids increases. "Negative air gap" is a term that designates a method of void elimination promoted by overlapping the rasters, as demonstrated in Fig. 3(e, f). In reality, decrease of the layer height leads to a reduction of voids size.

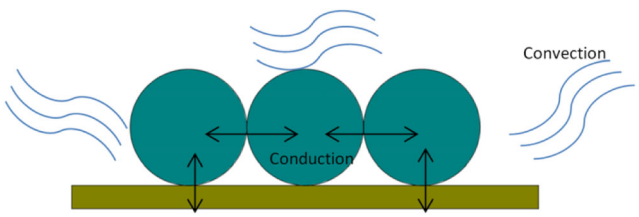

Fig. 2 A schematic of heat transfer mechanisms in deposition stage: conduction between rasters and layers and bed, and convection between rasters and ambient

Filling Percentage This parameter determines the interior solidity of the model. In principle, the outer layers of the part (shell) is printed solid and the inner sections are decided to printed partially filled, depending on the application; a fully solid printing will yield a stronger part in expense of material usage and printing time. Amount of infill is crucial in reducing material usage and total cost. Figure 4 illustrates the schematic of the produced parts with 0, 25, 50, 75, and 100 filling percentages.

Fill Pattern This parameter represents the way that deposition procedure is carried out. It is possible to carry different filling patterns such as line, rectilinear, grid, triangle, star, cubic, concentric, honeycomb, 3D honeycomb, hilbert curve, Archimedean chords, and octagram spiral. Figure 5 describes these known patterns and their arrangements in each layer. The filing pattern affects the strength by arranging rasters in a way that influences heat transfer. The consequence is that the bonding between rasters and layers will be affected. The filling pattern also determines the raster orientation.

The mechanical strength of the final printed product can be justified by considering the raster orientation and thermal history, assuming all other conditions are unchanged. As mentioned earlier, the maximum strength is achieved when the rasters and loading are in the same direction. If the rasters direction is considered as the main contributor to the strength, the "line filling pattern" is expected to yield the highest tensile strength, as manifested in a unidirectional tensile test. If the length of the printed part is larger than its width it can be expressed that the concentric pattern partially provides the same feature. On the other hand, if thermal history is considered as the key factor for the strength, the printing pattern with the shortest deposition distance, at the layers, would yield the highest strength. As explained earlier, this is due to the higher heat transfer between rasters that, consequently, promotes the fusion of molecules at the contact zones, and thus, strengthening the bonds between the rasters. With this hypothesis, hilbert curve would provide a

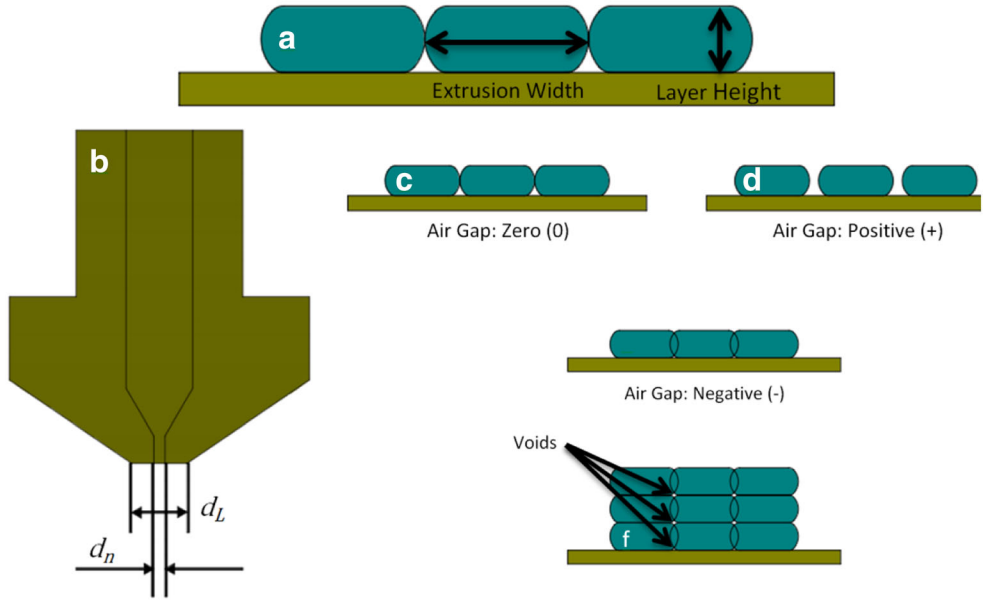

Fig. 3 The concept of layer height, extrusion width, inner and outer diameter of nozzle, and air gap for small layer height

higher strength because the deposition path in this pattern is the shortest, provided that the rasters are in contacts with each other's (meaning that this could be well manifested at a higher fill percentage, specifically 100%). In order to better understand the effect of filling pattern on thermal history and as a result of the bonding quality and mechanical properties, the temperature variations in fused deposition modeling process is discussed in detail in the next section.

Heat Transfer in Fused Deposition Modeling Process

If assumed that a raster with a fixed length is deposited on the table or the previous layer; so in order to calculate the temperature in different points of the raster one element can be considered and perform a thermal analysis on it. A simplified model of the temperature distribution in the deposited filament has been addressed by Bellehumeur et al. [10]. Suppose that an element is considered as shown in Fig. 6. If assumed the cross-section of the deposited raster and the element is a rectangle, neglecting the rounded corners of the deposited raster will have no effect on the cross-sectional size and the analysis.

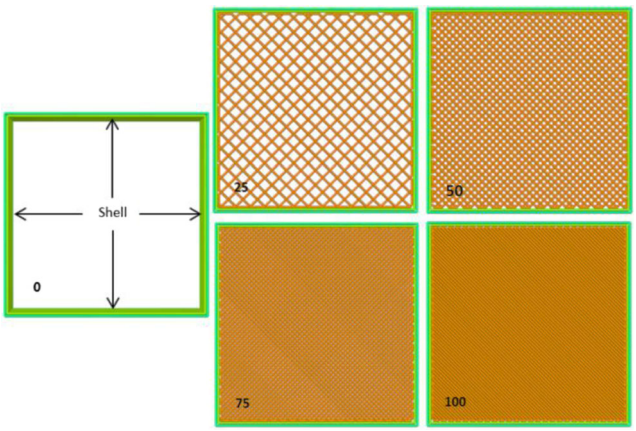

Fig. 4 Schematics of different filling percentage 0, 25, 50, 75, and 100%

Assumed that the origin of the coordinate is in the nozzle output and heat transfer of raster is one-dimensional and in the x-axis direction. Also, the temperature at the starting point of the process is known and measurable after a certain amount of mileage. As is clear, the length of the element is dx, the width of the element is equal to the extrusion width (w) and the thickness of the element is equal to the layer height (h). If it is assumed that the heat transfer from the bottom of the element to the table or the previous layer equals the heat transfer of the surrounding environment, it can be written according to the energy balance for the element [23]:

$$q_x - q_{x+dx} - h_{Conv} A_{Conv} (T - T_\infty) = \rho C V (\partial T / \partial t) \quad (1)$$

In this equation, q_x is the input conduction heat transfer to the element, q_{x+dx} is the output conduction heat transfer from the element, h_{Conv} is the convection heat transfer coefficient, A_{Conv} is the sections in contact with the air of the environment, T is the temperature at each point, T_∞ is the environment temperature, ρ is the density, C is the specific heat capacity, V is the volume of the element and $\partial T/\partial t$ is the temperature change per time. On the other hand it is clear [23]:

$$q_x = -kA(\partial T / \partial x) \quad (2)$$

$$q_{x+dx} = -kA(\partial T / \partial x) + (\partial(-kA(\partial T / \partial x))/\partial x)dx \quad (3)$$

In these equations k is the thermal conductivity coefficient, A_{Cond} is the cross-section of the element and $\partial T/\partial x$ is the

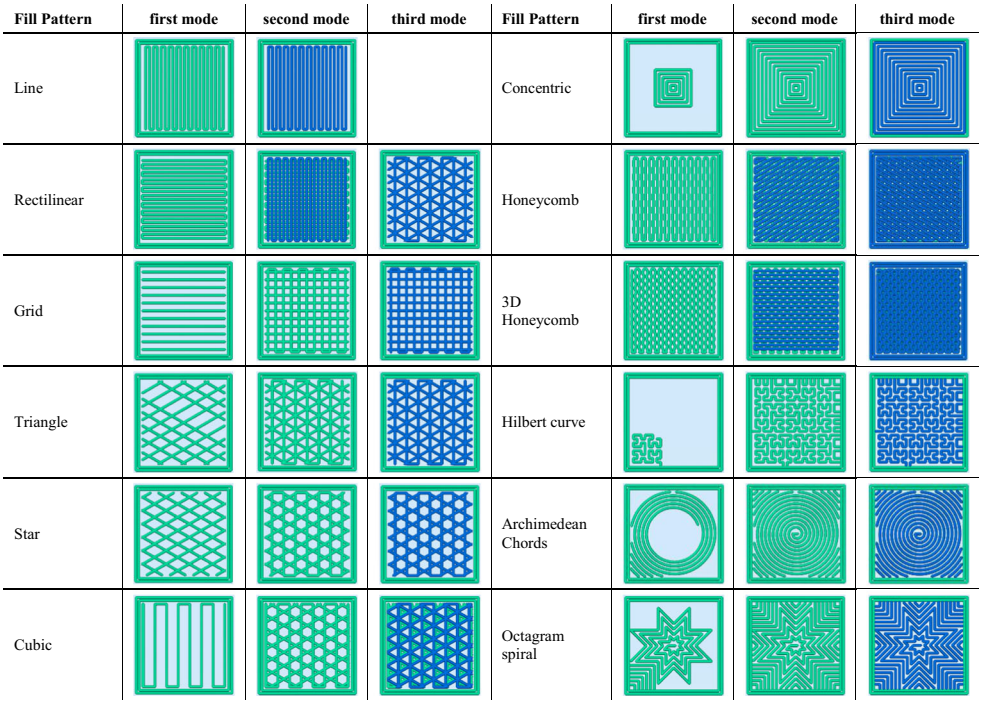

Fig. 5 Different configurations of filling pattern

temperature variation relative to location. Of course it is assumed that "k" is not a function of the temperature and it is unchanging. By inserting equations. (2) and (3) in equation (1) and simplifying:

$$kwh\left(\partial^2 T/\partial^2 x\right) - h_{Conv}(2h + 2w)(T - T_\infty) = \rho Cwh(\partial T/\partial t) \quad (4)$$

Since in the fused deposition modeling, the nozzle velocity is constant and equals v then [10]:

$$\partial T/\partial t = (\partial T/\partial x)(\partial x/\partial t) = v(\partial T/\partial x) \quad (5)$$

Finally, equation (4) after simplification equals:

$$d^2T/d^2x - a(dT/dx) - b(T - T_\infty) = 0 \quad (6)$$

In this equation:

$$\begin{aligned} a &= \rho Cv/k \\ b &= (2h_{Conv}(h + w))/kwh \end{aligned} \quad (7)$$

If the temperature at $x = 0$ is equal to the nozzle temperature and at a specified distance from the nozzle is known, the answer of equation (6) is equals to:

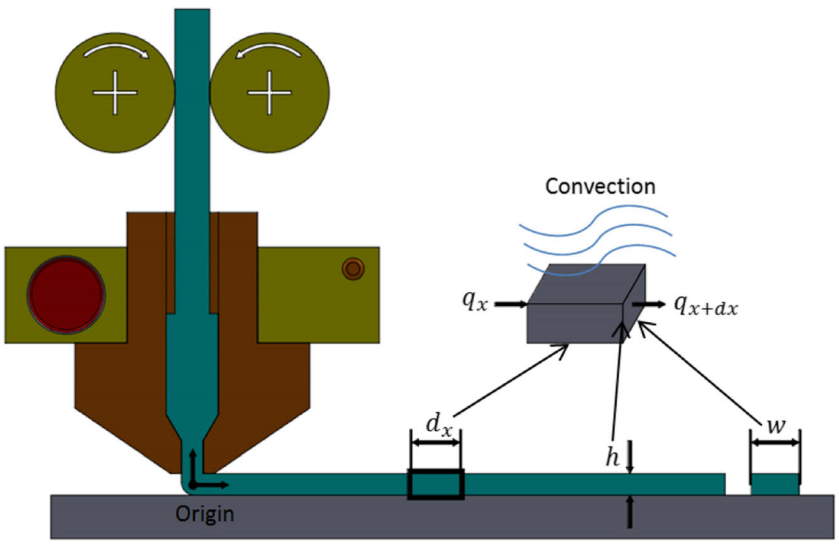

Fig. 6 The considered element for thermal analysis

$$T(x) = (T_N - T_\infty)e^{(x/2)\left(a-\sqrt{a^2+4b}\right)} + T_\infty \quad (8)$$

Using the values in Table 1, the answer of equation is equal to:

$$T(x) = 193e^{-10.92x} + 27 \quad (9)$$

In Fig. 7(a), the temperature variations in deposited raster based on the motion of the nozzle is shown. As shown in Fig. 7(a), as nozzle moves away the temperature of raster decreases. Therefore, regarding filling pattern such as the line and concentric patterns (Fig. 7(b)), due to the temperature decrease, the bonding between the rasters is weak. In a pattern such as the hilbert curve, in which the nozzle runs very short distances (Fig. 7(c)), the bonding between the rasters is strong since there is no great temperature drop, and at movement distances this pattern is less than 5 degrees.

Design of Experiment

The selected filling patterns, as the main parameter of study in this research work, were concentric, rectilinear with the raster angles of ±45, hilbert curve, and honeycomb (Fig. 8). The reason for selecting these filling patterns is that they can be well examined for the rasters orientation and the bonding between them. In the concentric filling pattern, all rasters are placed along with the load. This pattern is similar to the line pattern, but since the print path is concentric, the amount of distortion obtained in this pattern is less and more uniform than the line pattern. The rectilinear pattern with +45/− 45 raster angles is selected due to the fact that the layers are printed perpendicularly and they can fill the blank spaces created on the edges of the rasters and provide a higher strength than the 0/90 raster angles. In addition, patterns like grid, Triangle, star, and cubic in filling percentage of 100, have a rectilinear pattern with +45/− 45 raster angles. Honeycomb filling pattern has also been used in the construction of various structures and has therefore been investigated. In hilbert curve filling pattern, since the nozzle performs a print operation at smaller distances than other patterns, the bonding between the rasters is therefore stronger than other patterns. The filling percentage of 20, 50, and 100 were also considered as variable parameter. These two parameters indirectly responsible for rasters orientation and void presence, the effects of which were discussed earlier. The other processing parameters were maintained unchanged (Table 2). Tensile and flexural test samples were printed according to ASTM D638, type IV, and ASTM D790, respectively, to measure tensile and flexural strength/modulus. For each data point, five samples were printed to yield confident data.

Table 1 The values used to solve equation (8)

$T_N = 220^\circ C$
$T_\infty = 27^\circ C$
$v = 0.04\ m/s$
$\rho = 1250\ \mathrm{Kg/m^3}$
$h_{Conv} = 75\ w/m^{2^\circ}\mathrm{C}$ [10]
$C = 2060\ j/Kg^\circ\mathrm{C}$ [24]
$k = 0.195\ w/m^\circ\mathrm{C}$ [24]
$h = 0.2\ mm$
$w = 0.4\ mm$

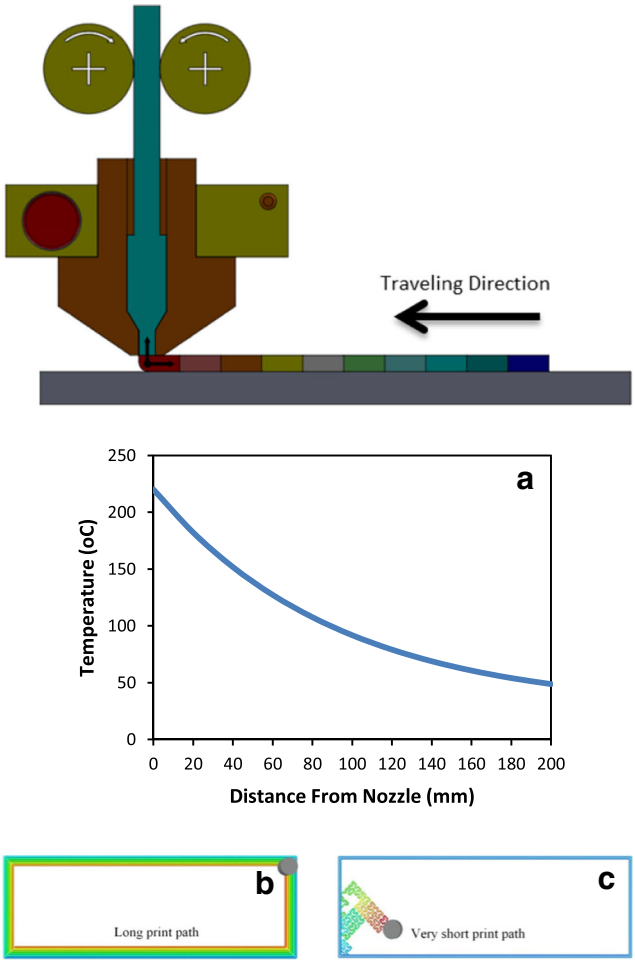

Fig. 7 (**a**) Diagram showing the effect of travel distance of nozzle on temperature of the deposited raster (**b**) concentric pattern; nozzle travels in a long distance before depositing the next raster. (**c**) hilbert curve pattern; nozzle travels in a very short distance before depositing the next raster

Material and Equipment

Poly-lactic Acid (PLA) filament of 1.75 mm in diameter, purchased from Digimaker, Canada, was used as the polymeric feedstock material for printing. A laboratory FDM 3D printer

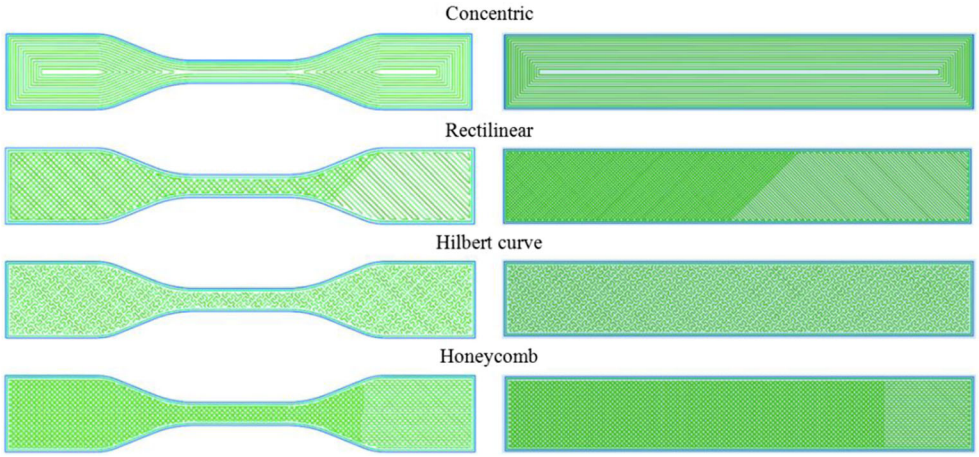

Fig. 8 Schematic of selected filling patterns with 100% fill percentage: concentric, rectilinear with the raster angles of ±45, hilbert curve, and honeycomb

with bed dimensions of 195x195x200 mm was employed. The bed temperature was set below100°C to compensate the lower heat transfer rate between the bed and the first layer, and between the following consecutive layers, this would promote the mass fusion at the contact surfaces that could strengthen the thermal bonding. Nozzle temperature was set at 220°C, as this could cause a drop in polymer viscosity, and lead to filling of voids throughout the polymeric matrix. Moreover, at this high initial temperature of rasters, a stronger bonding would be promoted. A universal tensile test machine (Santam STM-20, Iran) was used to measure tensile and flexural mechanical properties. Scanning electron microscopy was carried using an SEM (Prox-phenom, Netherlands), to examine the fractured surfaces of the printed samples after tensile and three point flexural tests, in terms of void presence and the bonding quality.

Results and Discussions

Tensile and flexural mechanical properties: Examples of stress–strain diagrams resulted from tensile tests are shown in Fig. 9, for filling percentages of 20, 50 and 100 and the examined filling patterns.

Table 2 Printing parameters

Parameter	Value
Nozzle diameter	0.4 *mm*
Air gap	−0.05 *mm*
Extrusion (bead) width	0.4 *mm*
Layer height	0.2 *mm*
Build direction	*XYZ*
Fill percentage	20, 50 *and* 100%
Print speed	40 *mm/s*
Infill/Perimeter Overlap	40%
Perimeter	2

The average and standard deviation values of the tensile strength for all the samples are presented in Fig. 10, vs. filling pattern and percentages.

Figure 10(a) indicates that concentric pattern promotes higher averaged tensile strengths at all filling percentages compared to the other examined filling patterns. Figure 10(b) depicts the same results of tensile strength vs. filling percentage. While at the filling percentages of 20 and 50, concentric pattern exhibits the highest strength, rectilinear and honeycomb patterns present almost similar strengths but both less than that of concentric one. Hilbert curve pattern offers the least strength at these filling percentages. With an increase in the filling percentage, tensile strength increases for all the examined filling patterns. The obvious reason is the increase in the polymer material content that can support further load. Surprisingly, at the filling percentage of 100, hilbert curve pattern presents a strength equivalent to that of the concentric pattern; though in this (Hilbert) pattern, the rasters are not aligned with the loading direction. This unique increase can be attributed to the strengthened bonding between the rasters, at the filling percentage of 100. It may be surmised that, with the filling percentages of 20 and 50, the rasters direction and the bonding between the layers are the determining factors for the final strength. But, with the filling percentage of 100, the bonding between rasters also comes into playing an important role in the final mechanical properties. In the hilbert pattern, since the nozzle travels mostly in short distances, before changing direction, the deposited raster experience much less temperature drop before coming into contact with the next adjacent deposited raster; referring to Fig. 7(c), at short travelling distance of nozzle, the raster temperature maintains high and a less temperature drop is experienced. As a result, the bonding between the adjacent rasters is stronger as the fusion at the raster surfaces is highly promoted. In this filling pattern, and with filling percentages of 20 and 50, the rasters are not aligned with the loading direction, and that is reason for showing the lowest strength

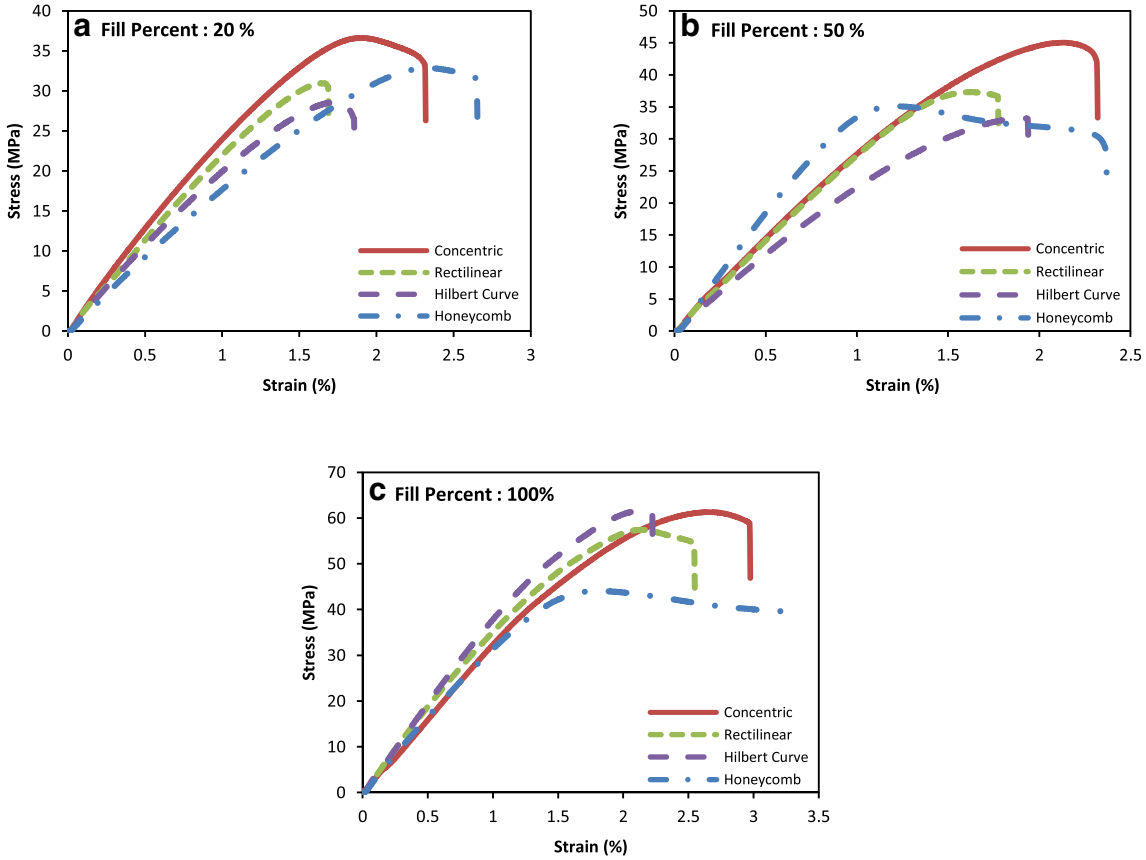

Fig. 9 Stress-strain diagrams obtained from the tensile test for samples with a fill percentage of (**a**) 20, (**b**) 50 and (**c**) 100%

among the other examined patterns. With the filling percentage of 100, a dense part is formed with strong bondings between the rasters and the layers (Fig. 11).

Conversely for honeycomb pattern, the increase in strength with the filling percentage of 100 is not comparable with those of other examined patterns (less increase). The reason is that even with the (nominal) set filling percentage of 100, rasters are not adhered in myriad of locations and thus a complete bonding between the rasters is not promoted in the honeycomb pattern due to the nature of nozzle movement and raster deposition (Fig. 12).

At the filling percentage of 100, the highest strength belongs to concentric and hilbert curve patterns, that are 62 MPa and 61 MPa, respectively.

Figure 13(a) shows tensile modulus for the examined filling patterns at the filling percentages of 20, 50 and 100. As shown in this figure, in every pattern, modulus increases as the filling percentage increases. Figure 13(b) depicts the same results vs. filling percentage. Similar to the results for the strength, the highest modulus is obtained when concentric filling pattern is employed, at all filling percentages. By adding that, an exceptional increase in modulus is experienced

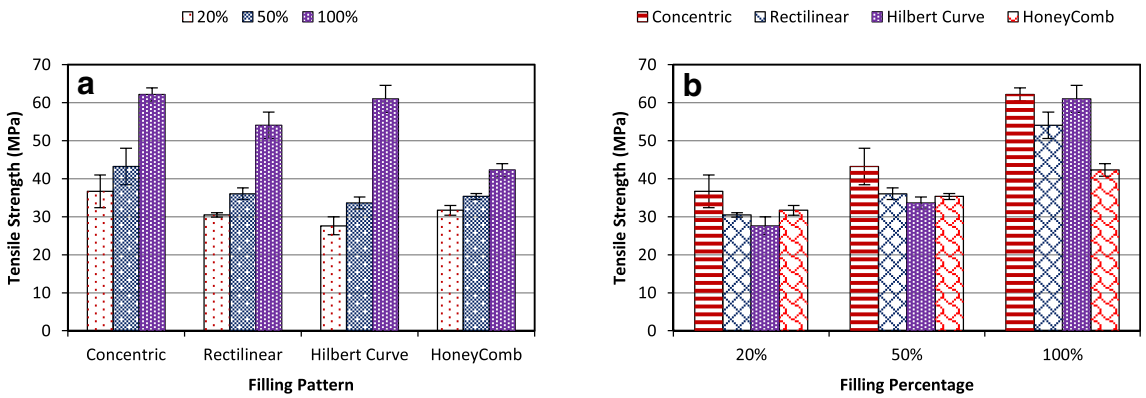

Fig. 10 Tensile strengths of the printed specimens vs. (**a**) filling pattern and (**b**) filling percentage

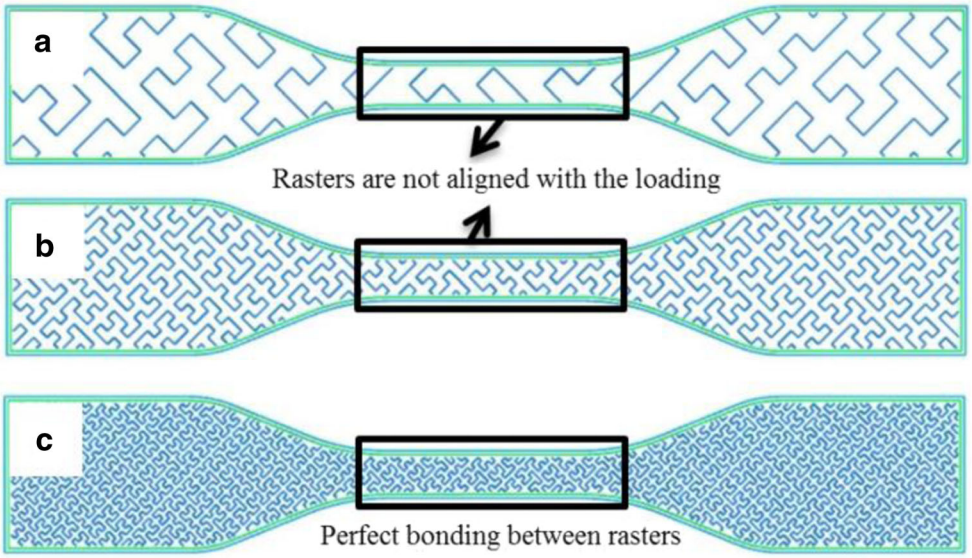

Fig. 11 Hilbert curve filling pattern in the filling percentage of (**a**) 20, (**b**) 50 and (**c**) 100

with the hilbert curve pattern, at the filling percentage of 100. Similar above-mentioned reasons can be presented to justify this unique increase (strong bonding of the rasters due to the short nozzle traveling distances). As it can be seen, the maximum amounts of modulus for the filling percentage of 100 belong to the concentric pattern and hilbert curve, that are 3.48 GPa and 3.36 GPa, respectively. The assumed dominant effect of raster alignment with the loading direction is evident at the filling percentage of 20, as concentric pattern offers the highest modulus in the filling percentage of 50, all the patterns present an almost similar tensile modulus, but the hilbert curve pattern presents the lowest. The reason is that in this pattern and at this filling percentage, the rasters are deposited in a way that they do not present an efficient resistance against the applied load. At the filling percentage of 100, the amount of tensile modulus are almost the same; but for the concentric pattern due to the alignment of the rasters and the loading direction and for the hilbert curve pattern due to the strong bonding between the layers and rasters, the tensile modulus the highest.

For better understanding the effect of filling percentage on strength and tensile modulus, specific tensile strength and modulus were calculated and depicted in Fig. 14, for the examined filling patterns and percentages. As observed in the figure, the highest specific tensile strength values, at the filling percentages of 20 and 50, belong to the concentric pattern, and at the filling percentage of 100 are associated with both concentric and hilbert curve patterns. Interesting to note that the maximum specific tensile strength for concentric and honeycomb patterns occurs at the filling percentage of 20, and for the rectilinear and hilbert curves pattern occurs at the filling percentage of 100. It is notable that at the filling percentage of 20, both concentric and honeycomb patterns exhibited higher tensile strengths than those of the other two patterns (Fig. 10(b)). Another considerable result is that at the filling percentage of 100, the specific tensile strength is higher than that at the filling percentage of 50, for all the examined patterns except the honeycomb pattern. Honeycomb pattern is more susceptible to create small voids in the matrix that could yield a significant reduction in the specific tensile strength (SEM micrographs support this argument and will be discussed in the following section). The practical outcome of the results is that concentric pattern is by far superior to the other patters regardless of filling percentage. However, alternative selection could be rectilinear pattern at the low spectrum of filling percentages and hilbert curve at the high spectrum of filling percentages, when a high specific strength is the major governing criterion. The specific tensile modulus behavior is similar to that of the specific tensile strength, as evident in Fig. 14(c) and (d).

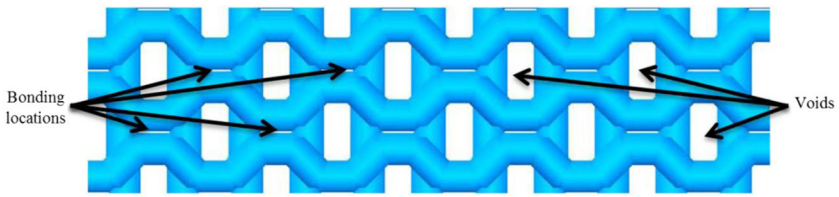

Fig. 12 Honeycomb filling pattern in filling percentage of 100; bonding between rasters and voids formation

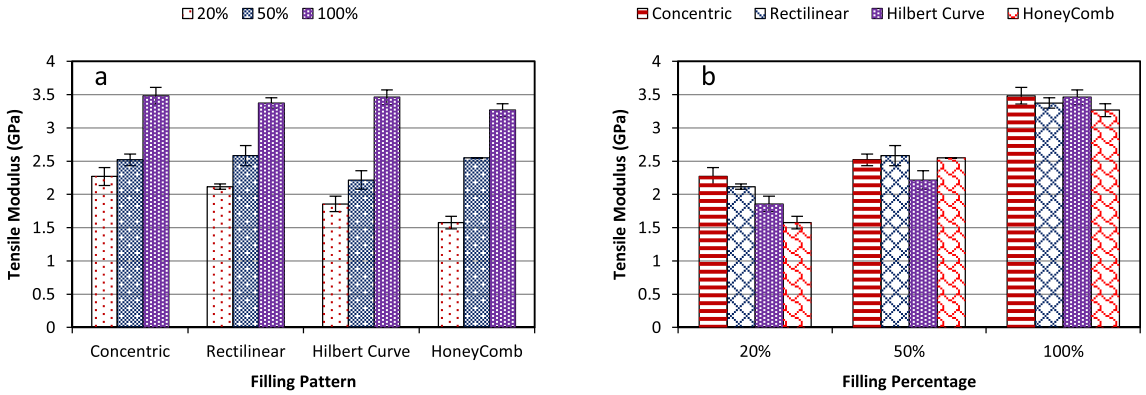

Fig. 13 Tensile modulus of the printed specimens vs. (**a**) filling pattern and (**b**) filling percentage

The stress–strain diagrams resulted from the three point flexural test are shown in Fig. 15 for the examined filling patterns and the filling percentages. The calculated averaged and standard deviations of flexural strength are depicted in Fig. 16. Similar results to those of tensile strengths have been observed for flexural strengths: concentric pattern exhibited the highest strength at all examined filling patterns, attributed to the rasters alignment with the loading direction. A remarkable increase in flexural strength is also observed for hilbert curve at the filling percentage of 100 which is consistent with the results obtained for the tensile strengths. As explained earlier, this could be justified by the strong bonding between the adjacent deposited

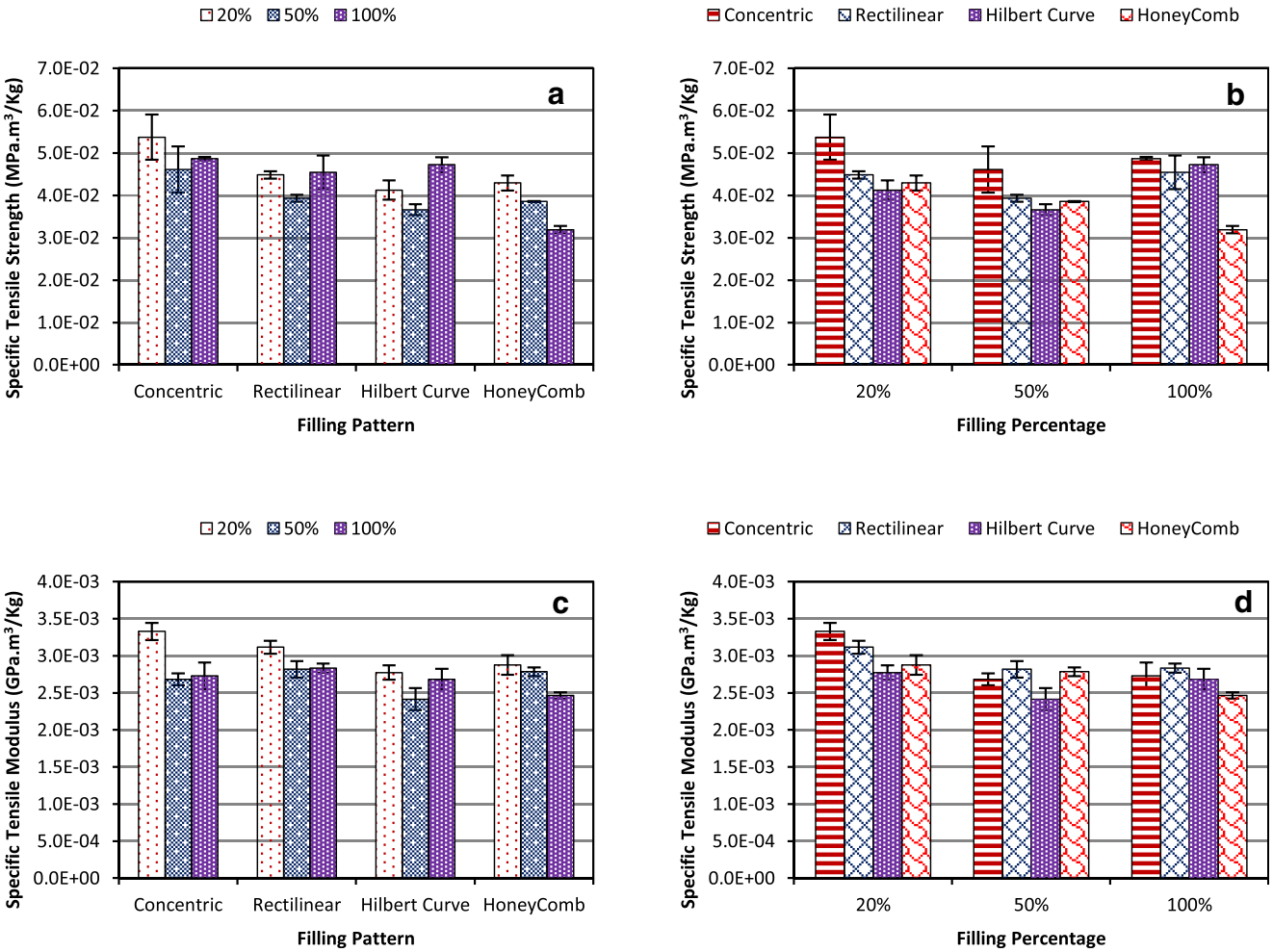

Fig. 14 Specific tensile strength of the printed specimens vs. (**a**) filling pattern and (**b**) filling percentage and Specific tensile modulus of the printed specimens vs. (**c**) filling pattern and (**d**) filling percentage

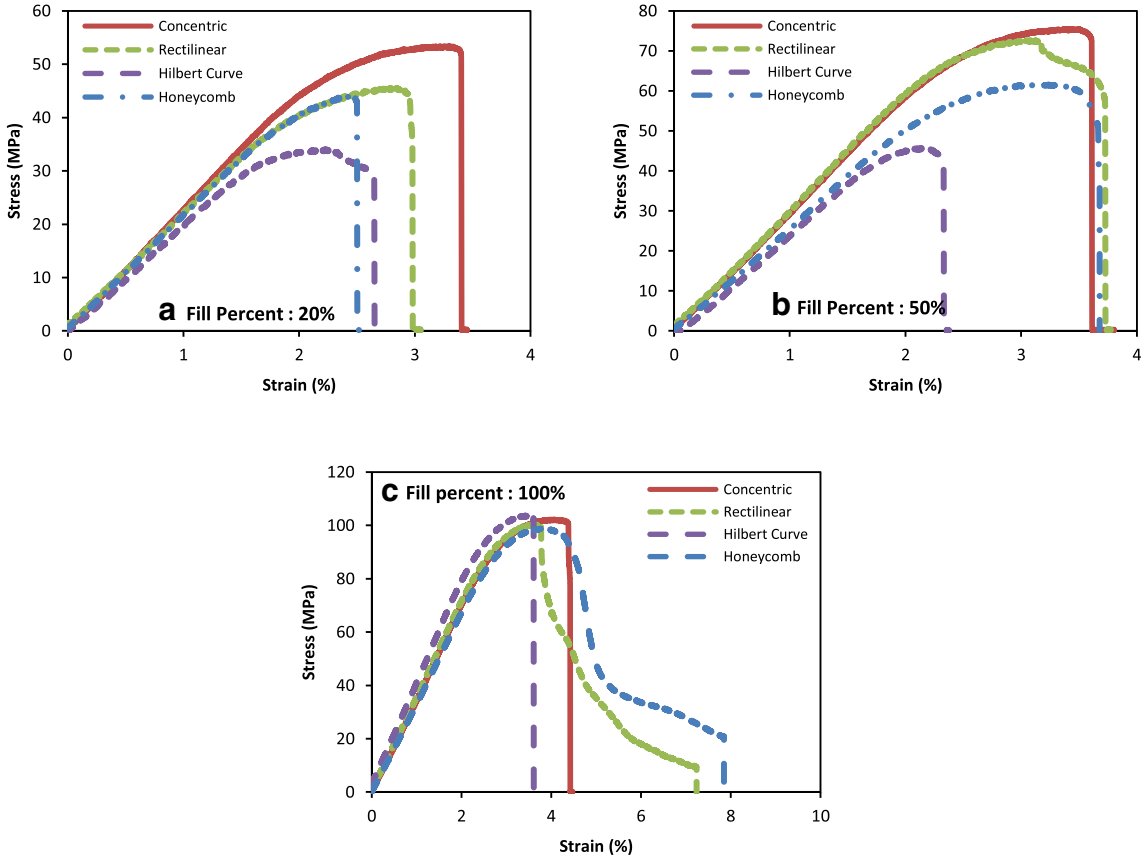

Fig. 15 Stress-strain diagrams obtained from the three point flexural test for samples with a fill percentage of (**a**) 20, (**b**) 50 and (**c**) 100%

rasters, where a high temperature is maintained due to the short travelling distances of the nozzle in hilbert curve pattern.

The flexural strength in the hilbert curve and concentric patterns is about 102 MPa at the filling percentage of 100. Figure 17 gives the results for flexural modulus against filling patterns and percentages. It is notable that the increase in flexural modulus for the hilbert curve pattern is dramatic, at 100% filling percentage, similar to that observed for the strength that is even higher than those of the other examined patterns; the maximum flexural modulus, 3.75 GPa, was obtained with this pattern.

The calculated values of specific flexural strength and modulus are shown in Fig. 18. The figure reveals that in the concentric filling pattern, the variation of the specific flexural strength in terms of filling percentages is insignificant. With regard to the rectilinear and honeycomb patterns, the specific flexural strength increases linearly with increasing filling percentages. Concerning the hilbert curve pattern, at the filling percentages of 20 and 50, the specific flexural strengths are almost the same, but increases significantly at the filling percentage of 100; this particular and notable behavior was not observed for the specific tensile strength. In addition, the

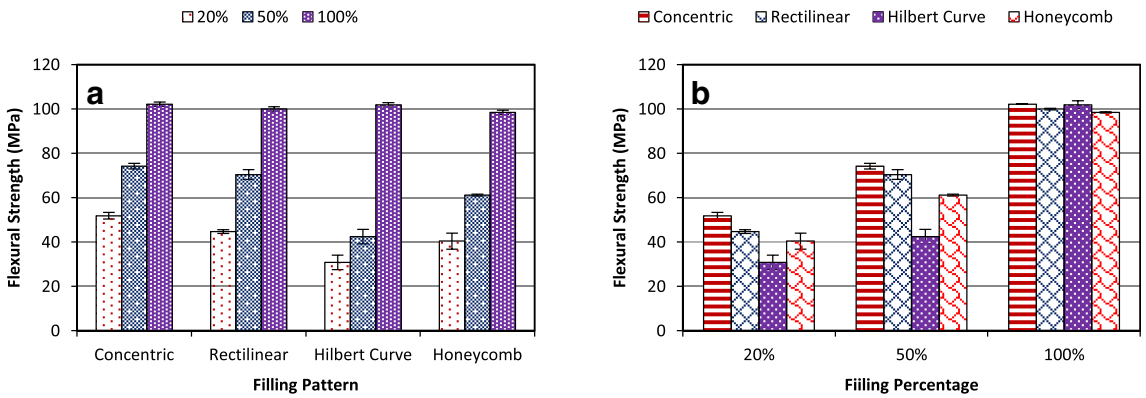

Fig. 16 Flexural strengths of printed specimens vs. (**a**) filling pattern and (**b**) filling percentage

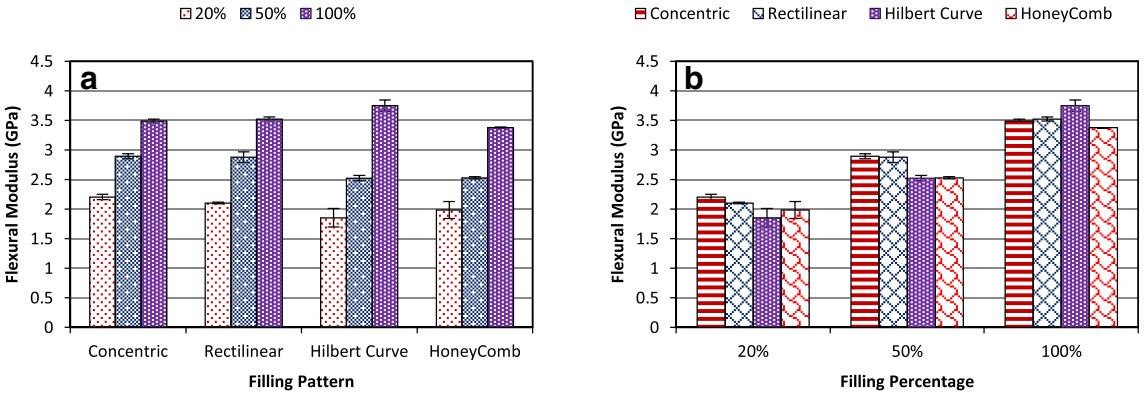

Fig. 17 Flexural modulus of printed specimens vs. (**a**) filling pattern and (**b**) filling percentage

highest specific flexural strength values were obtained at the filling percentage of 100; contrary to the results of specific tensile strength where the highest values were observed at the lowest filling percentage of 20. It can be concluded that, regardless of filling percentage, concentric pattern yields an optimum flexural strength. As an alternative, at low spectrum of filling percentages (here, 20 and 50), rectilinear pattern yields the desirable flexural strength-to-weight ratio (while hilbert curve is the least desirable), while at the highest spectrum of filling percentages, hilbert curve is the best alternative. The results of the specific flexural modulus indicate that with increasing the filling percentage, the specific flexural modulus decreases

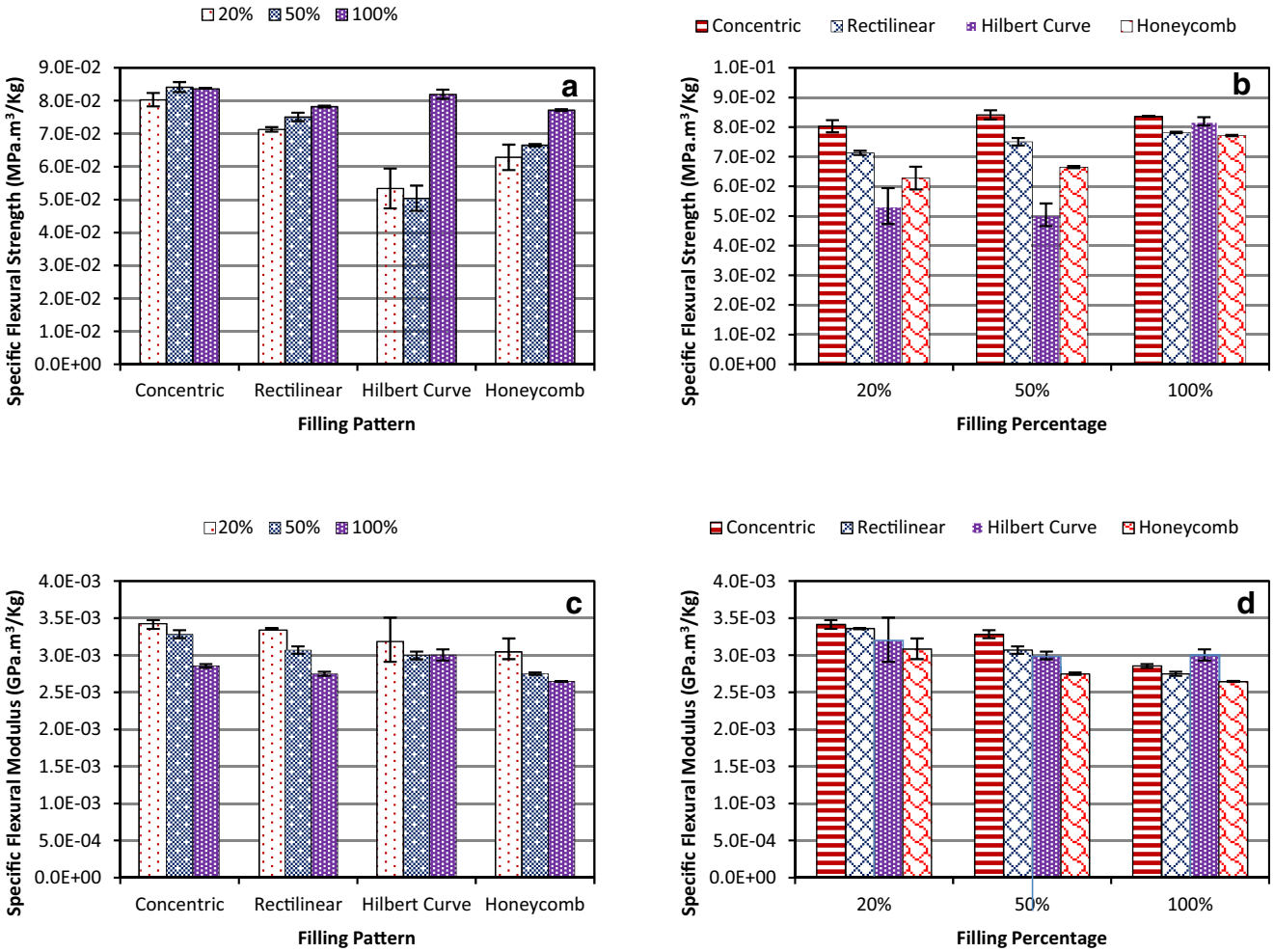

Fig. 18 Specific flexural strength of the printed specimens vs. (**a**) filling pattern and (**b**) filling percentage and Specific flexural modulus of the printed specimens vs. (**c**) filling pattern and (**d**) filling percentage

slightly, fairly similar to those of specific tensile strength; that means the maximum values of the specific flexural modulus are obtained at the lowest spectrum of filling percentages (here, 20). Furthermore, at the filling percentage of 100, hilbert curve pattern provides the highest specific flexural modulus. In overall, it can be said that specific flexural (and also tensile) modulus is less sensitive to the filling pattern and percentages. That is because the modulus is measured at the elastic portion of the stress-strain curve and is not affected by the voids and defects, in contrast to the strength.

Morphology: the justification of the variations in mechanical properties given above can be evaluated via examining the SEM micrographs of the fractured surfaces. Figures 19 and 20 reveal the microstructures of the fractured samples of tensile and flexural tests, respectively, with the filling percentage of 100.

As evident in Fig. 19, while voids are present in all samples, but for concentric and hilbert curve filling patterns, the number and sizes are minimized, indicating a stronger and efficient bonds between the rasters. This leads to a higher strength, as manifested in the results obtained from the mechanical tests. It was shown earlier that concentric pattern exhibited the highest strengths, both tensile and flexural. Also the micrograph associated with the hilbert curve (Fig. 19(c)) explains the remarkable increase in tensile strength at the filling percentage of 100. It is evident that the textures of the fracture surfaces are highly integrated. It is reasonable to assert that this could be mainly possible when the rasters are at a high temperature to promote desirable fusion and, consequently, to yields an integrated matrix. It is also evident that the voids are remarkably larger for the honeycomb pattern and the bonding between rasters is undesirable that explains the inferior mechanical properties of the printed samples with this pattern, at the filling percentage of 100 (Fig. 12).

Examples of SEM micrographs for the fractured surfaces of flexural test specimens are shown in Fig. 20. Similar to the tensile test specimens, concentric and hilbert curve pattern

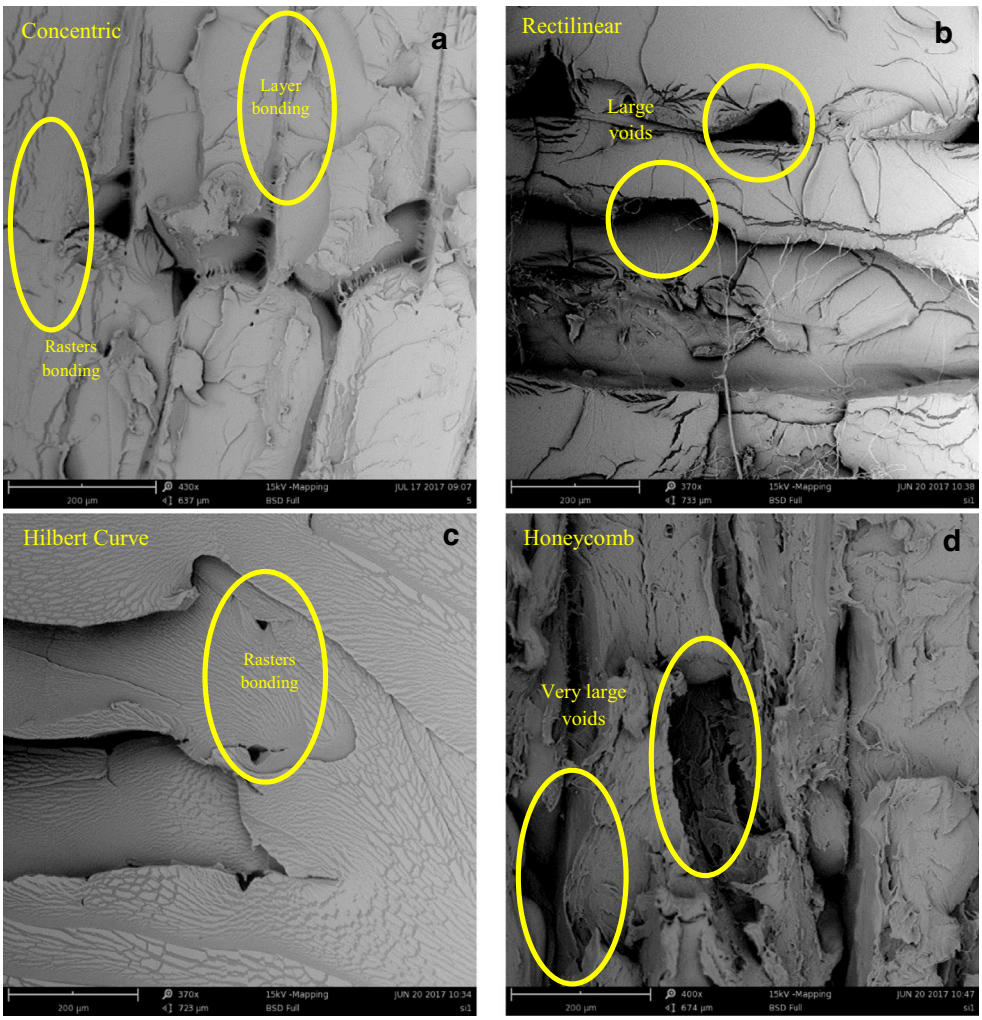

Fig. 19 SEM images of the fractured cross-section of tensile test specimens; (**a**) concentric pattern showing tiny voids, (**b**) rectilinear pattern showing large voids, (**c**) hilbert curve showing a low number of tiny voids, and (**d**) honeycomb showing a large number of large voids

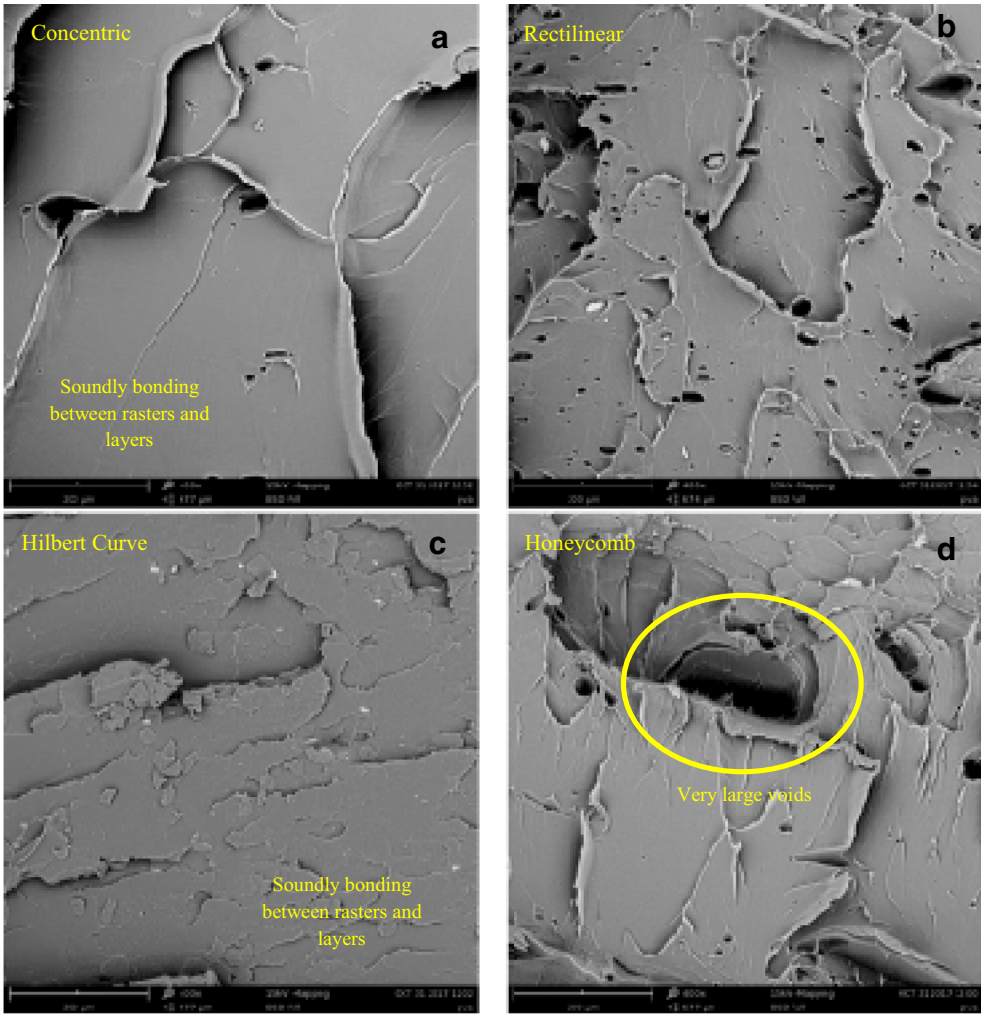

Fig. 20 SEM images of the fractured cross-section of flexural test specimens; (**a**) concentric pattern showing a low number of tiny voids, (**b**) rectilinear pattern showing large number of voids, (**c**) hilbert curve showing a highly integrated texture, and (**d**) honeycomb showing large voids

present the most desirable structures; though, the hilbert curve indicates almost a flawless texture. The micrographs manifest the strong bonding between rasters for concentric pattern and especially for hilbert curve pattern at the filling percentage of 100 that sound entirely desirable. This explains the competitiveness of hilbert curve with concentric pattern at the filling percentage of 100, as evident in the results of flexural test. The presence of large voids for the honeycomb pattern justifies the inferior flexural properties of the printed samples with this pattern with respect to the other examined patters, at the filling percentage of 100 (Fig. 20(a)).

Conclusions

The experimental study presented in this paper contributes to understanding the effect of filling pattern and percentage (infill percentage) on the mechanical properties of 3D printed parts in fused deposition modeling (FDM) method. The effect of different filling patterns and the infill percentages on the tensile and flexural strengths was investigated, with emphasis on rasters orientation, rasters bonding, and void formation. Concentric, hilbert curve, rectilinear, and honeycomb filling patterns at filling percentages of 20, 50 and 100% were examined. Results obtained from this study conclude the followings:

- Concentric pattern resulted in the highest mechanical properties (tensile and flexural strengths) that can be attributed to the alignment of rasters with the loading direction.
- Although, the higher filling percentages yielded the higher values in both tensile and flexural strength and modulus, this is not so obvious when taking the weight into account. The results indicate that the specific tensile and flexural modulus is the largest at the lowest filling percentage (here, 20). The specific tensile strength is the highest at this filling percentage except for hilbert curve.

- The printed specimens with the hilbert curve resulted in inferior properties at the low filling percentages (here 20 and 50). However, a dramatic increase in the tensile and flexural strengths was observed with the filling percentage of 100, makes it superior to the rectilinear and honeycomb patterns and equivalent to the concentric pattern.
- Honeycomb was found to be the least favorite at the filling percentage of 100, although it gave rise to better properties at the low filling percentage.
- SEM micrographs indicated the low number of tiny voids for both concentric and hilbert curve patters justifying the higher mechanical properties of the printed samples with these patterns at the highest filling percentage (here, 100). The presence of large voids in the printed specimen with the honeycomb pattern is the reason for their lowest strengths at this filling percentage (100).
- An analysis of thermal history in rasters suggests that when rasters are printed at short distances (such as in hilbert curve), a high temperature is maintained and thus a strong bonding between the adjacent rasters is developed due to a better fusion. This results in a matrix with less flaws, as evident in the SEM micrographs, and consequently a dramatic increase of the samples printed with hilbert curve pattern, at the high filling percentage.

Compliance with Ethical Standards

Conflict of Interest The authors declare that they have no conflict of interest.

Publisher's Note Springer Nature remains neutral with regard to jurisdictional claims in published maps and institutional affiliations.

References

1. Shaffer S, Yang K, Vargas J, Di Prima MA, Voit W (2014) On reducing anisotropy in 3D printed polymers via ionizing radiation. Polymer 55(23):5969–5979
2. Guo N, Leu MC (2013) Additive manufacturing: technology, applications and research needs. Front Mech Eng 8(3):215–243
3. Mostafa N, Syed HM, Igor S, Andrew G (2009) A study of melt flow analysis of an ABS-iron composite in fused deposition modelling process. Tsinghua Sci Technol 14:29–37
4. Goyanes A, Buanz AB, Basit AW, Gaisford S (2014) Fused-filament 3D printing (3DP) for fabrication of tablets. Int J Pharm 476(1):88–92
5. Mannoor MS, Jiang Z, James T, Kong YL, Malatesta KA, Soboyejo WO, Verma N, Gracias DH, McAlpine MC (2013) 3D printed bionic ears. Nano Lett 13(6):2634–2639
6. Li D, Feng X, Liao P, Ni H, Zhou Y, Huang M, Li Z, Zhu Y (2014) 3D reverse modeling and rapid prototyping of complete denture. Frontier and Future Development of Information Technology in Medicine and Education. Springer: 1919–1927
7. Hudson SE (2014) Printing teddy bears: a technique for 3D printing of soft interactive objects. Proceedings of the SIGCHI Conference on Human Factors in Computing Systems. ACM, pp 459–468
8. Serizawa R, Shitara M, Gong J, Makino M, Kabir MH, Furukawa H (2014) 3D jet printer of edible gels for food creation. Proceedings of SPIE Smart Structures and Materials Nondestructive Evaluation and Health Monitoring:90580A-90580A
9. Akhoundi B, Behravesh AH, Bagheri Saed A (2018) Improving mechanical properties of continuous fiber-reinforced thermoplastic composites produced by FDM 3D printer. J Reinf Plast Compos. https://doi.org/10.1177/0731684418807300
10. Bellehumeur C, Li L, Sun Q, Gu P (2004) Modeling of bond formation between polymer filaments in the fused deposition modeling process. J Manuf Process 6(2):170–178
11. Sun Q, Rizvi G, Bellehumeur C, Gu P (2008) Effect of processing conditions on the bonding quality of FDM polymer filaments. Rapid Prototyp J 14(2):72–80
12. Ahn S-H, Montero M, Odell D, Roundy S, Wright PK (2002) Anisotropic material properties of fused deposition modeling ABS. Rapid Prototyp J 8(4):248–257
13. Panda SK, Padhee S, Anoop Kumar S, Mahapatra S (2009) Optimization of fused deposition modelling (FDM) process parameters using bacterial foraging technique. Intell Inf Manag 1(02):89
14. Rayegani F, Onwubolu G (2014) Fused deposition modelling (FDM) process parameter prediction and optimization using group method for data handling (GMDH) and differential evolution (DE). Int J Adv Manuf Technol 73
15. Tymrak B, Kreiger M, Pearce JM (2014) Mechanical properties of components fabricated with open-source 3-D printers under realistic environmental conditions. Mater Des 58:242–246
16. Melenka GW, Schofield JS, Dawson MR, Carey JP (2015) Evaluation of dimensional accuracy and material properties of the MakerBot 3D desktop printer. Rapid Prototyp J 21(5):618–627
17. Torres J, Cotelo J, Karl J, Gordon AP (2015) Mechanical property optimization of FDM PLA in shear with multiple objectives. Jom 67(5):1183–1193
18. Baich L, Manogharan G, Marie H (2015) Study of infill print design on production cost-time of 3D printed ABS parts. Int J Rapid Manuf 5(3–4):308–319
19. Fernandez-Vicente M, Calle W, Ferrandiz S, Conejero A (2016) Effect of infill parameters on tensile mechanical behavior in desktop 3D printing. 3D Print Add Manufact 3(3):183–192
20. Dawoud M, Taha I, Ebeid SJ (2016) Mechanical behaviour of ABS: an experimental study using FDM and injection moulding techniques. J Manuf Process 21:39–45
21. Wang J, Xie H, Weng Z, Senthil T, Wu L (2016) A novel approach to improve mechanical properties of parts fabricated by fused deposition modeling. Mater Des 105:152–159
22. Mohamed OA, Masood SH, Bhowmik JL (2017) Experimental investigation of time-dependent mechanical properties of PC-ABS prototypes processed by FDM additive manufacturing process. Mater Lett 193:58–62
23. Holman JP (2001) Heat transfer, eighth SI metric edition. Mc Gran–Hill Book Company
24. Farah S, Anderson DG, Langer R (2016) Physical and mechanical properties of PLA, and their functions in widespread applications—a comprehensive review. Adv Drug Deliv Rev 107:367–392